Biophysical Journal Volume 75 August 1998 1107–1116

A Unified Resistor-Capacitor Model for Impedance, Dielectrophoresis, Electrorotation, and Induced Transmembrane Potential

Jan Gimsa and Derk Wachner
Institut für Biologie, Humboldt-Universität zu Berlin, Berlin, Germany

ABSTRACT Dielectric properties of suspended cells are explored by analysis of the frequency-dependent response to electric fields. Impedance (IMP) registers the electric response, and kinetic phenomena like orientation, translation, deformation, or rotation can also be analyzed. All responses can generally be described by a unified theory. This is demonstrated by an RC model for the structural polarizations of biological cells, allowing intuitive comparison of the IMP, dielectrophoresis (DP), and electrorotation (ER) methods. For derivations, cells of prismatic geometry embedded in elementary cubes formed by the external solution were assumed. All geometrical constituents of the model were described by parallel circuits of a capacitor and a resistor. The IMP of the suspension is given by a meshwork of elementary cubes. Each elementary cube was modeled by two branches describing the current flow through and around the cell. To model DP and ER, the external branch was subdivided to obtain a reference potential. Real and imaginary parts of the potential difference of the cell surface and the reference reflect the frequency behavior of DP and ER. The scheme resembles an unbalanced Wheatstone bridge, in which IMP measures the current-voltage behavior of the feed signal and DP and ER are the measuring signal. Model predictions were consistent with IMP, DP, and ER experiments on human red cells, as well as with the frequency dependence of field-induced hemolysis. The influential radius concept is proposed, which allows easy derivation of simplified equations for the characteristic properties of a spherical single-shell model on the basis of the RC model.

INTRODUCTION

Passive electrical properties of biological materials have always been of special interest, and research in this field is currently growing. Whereas in the past advantage was taken of the advancement of electronic technologies to increase resolution and sensitivity for basic research, the growing concern about the possible health effects of electromagnetic fields has become a driving force for research. Investigations of electrical properties contributed to our notion of the structure of biological matter. Already in 1925 Fricke's impedance (IMP) measurements proved that biological cells are covered by a thin, insulating membrane (Fricke, 1925). The IMP of biological material is characterized by a variety of characteristic frequency-dependent changes. These changes are based on the fact that permittivity contributions of certain relaxation processes that follow the external field at lower fequencies disperse at higher ones. Consequently, the permittivity of biological material drops over some frequency decades by orders of magnitude (Pethig and Kell, 1987; Schwan and Takashima, 1993). The aim of research was to assign the measured dispersions mediating the permittivity decrease to certain biological structures on different hierarchical levels and to classify the contributing processes (Fricke, 1925, 1953; O'Konski, 1960; Ackmann and Seitz, 1984; Ballario et al., 1984; Pethig and Kell, 1987; Bao et al., 1992; Schwan and Takashima, 1993; Lisin et al., 1996). For the classification of dispersions, two different approaches were chosen: the dispersions were sorted according to their physical nature, e.g., as Maxwell-Wagner and Debye dispersions, or according to the frequency range in which they occur. Whereas Maxwell-Wagner dispersions are based on the structure of the material, Debye dispersions are caused by the frequency dependence of the orientation of molecular dipoles. A classification according to frequencies originally yielded a scale in which dispersions with increasing frequencies were assigned to an α, β, or γ range. At that time it was assumed that well-defined processes are responsible for a certain dispersion range. Later the ranges were subdivided, e.g., the β range into $\beta 1$ and $\beta 2$. Furthermore, processes based on a certain mechanism that were originally assigned to a certain dispersion range may be observed in another frequency range, e.g., Debye dispersions of molecules of various sizes.

Despite their low frequency, analysis of α-dispersions in the frequency range below 1 kHz is especially difficult. Many different processes may influence the measurements, such as electrode polarizations, even electrolytic processes, hydrodynamic relaxations of electroosmotically induced convections within the measuring chamber and around the particles, as well as particle electrophoresis. The difficulty is that these phenomena are hard to separate and concurrently influence suspension medium and particles. When field-induced particle movements are registered, especially below 100 Hz, the suspension medium can no longer be considered a reference system. Despite these difficulties, an advance in this field was recently achieved (Georgiewa et al., 1998).

The β-dispersion range is best characterized. For biological cells its main components are Maxwell-Wagner disper-

Received for publication 13 January 1998 and in final form 20 May 1998.
Address reprint requests to Dr. Jan Gimsa, Institut für Biologie, Humboldt-Universität zu Berlin, Invalidenstrasse 42, D-10115 Berlin, Germany. Tel.: +49-30-2093-8494; Fax: +49-30-2093-8520; E-mail: jan=gimsa@rz.hu-berlin.de.

0006-3495/98/08/1107/10 $2.00

sions, i.e., the dispersions of structural polarizations as those of the cytoplasmic membrane or of internal membrane systems, as well as the polarization of the cytoplasm. Some authors classify the dispersions of the plasma membrane and internal membrane structures as $\beta 1$ and $\beta 2$ dispersions, respectively (Asami and Yonezawa, 1996). In the following we will refer to the dispersion of the cytoplasmic membrane and the cytoplasmic conductivity effects as $\beta 1$ and $\beta 2$ dispersions, to stress their different qualities. It is clear that the structural dispersions may be influenced by other processes like surface conductance (Fuhr and Kuzmin, 1986; Paul et al., 1993), membrane transport processes (Donath et al., 1990; Sukhorukov and Zimmermann, 1996), or dipole relaxations of macromolecules (Pethig and Kell, 1987; Gimsa et al., 1996). Because of the low sensitivity, IMP measurements did not allow detailed investigations of all relevant processes under physiological conditions.

In the γ range above 100 MHz, quick dissociation-association relaxations or Debye dispersions of small molecules or charged groups must be expected. Dispersions in pure protein suspensions are generally of the same quality and can be observed as a decrease in the dielectric constant (the dielectric decrement; Takashima and Asami, 1993). The dielectric properties of proteins are believed to be important for their physiological function, such as protein-protein association or interaction with charged ligands (O'Konski, 1960; Takashima and Asami, 1993). It has been known for a long time that in cell suspensions the protein dispersions are masked by the stronger structural β dispersions (Schwan, 1957). Therefore, cytoplasmic proteins were predominantly investigated after cell lysis or in cell-free suspensions (Pauly and Schwan, 1966; Takashima and Asami, 1993). The γ dispersion over 10 GHz was assigned to free water (Pethig and Kell, 1987). Dispersions between 1 and 10 GHz were assigned to bound water (δ-dispersion). Up to now technical problems hindered the access of single-cell spectroscopy to this frequency range by dielectrophoresis (DP) and electrorotation (ER).

Generally, IMP and the single-cell methods yield the same information on dielectric cell properties (Wang et al., 1993). In DP and ER, the translation and rotation of single cells in an inhomogeneous and rotating external field, respectively, are analyzed. The different motions in DP and ER depend on the different spatial properties of the field determining the interaction with the induced dipole moment. In DP, cells or particles move toward or away from regions of high field, depending on their polarizability relative to that of the suspension medium. Frequency-dependent changes of the DP force are mediated by dispersions of the cell's polarizability relative to that of the medium. In ER the rotating field induces a cell dipole moment that rotates at the angular frequency of the external field. Any dispersion process causes a spatial phase shift of the external field vector and the induced dipole moment, giving rise to a torque that causes individual cell rotation. The torque and therefore cell rotation are at maximum if the relaxation times of the dispersion process and external field frequency match. From the frequency dependencies of DP and ER, dielectric properties can be recalculated by applying appropriate models. Like models for IMP, models for multishell spherical, cylindrical, and ellipsoidal geometries are readily available (Pauly and Schwan, 1959; Crane and Pohl, 1972; Pohl, 1978; Pastushenko et al., 1985; Sauer and Schloegl, 1985; Fuhr et al., 1986; Paul and Otwinowski, 1991; Wang et al., 1993). In the field of biology, interesting applications of the methods are the determination, screening, or the pursuit of changes in membrane capacitance, membrane conductance, and cytoplasmic properties (Arnold and Zimmermann, 1982; Zimmermann and Arnold, 1983; Arnold et al., 1986; Geier et al., 1987; Georgiewa et al., 1989; Burt et al., 1990; Fuhr et al., 1990; Kaler and Jones, 1990; Gascoyne et al., 1995; Müller et al., 1990; Wang et al., 1994; Gimsa et al., 1991a,b, 1994, 1996; Hölzel, 1997). Ellipsoidal single-shell models have been applied to human red cells (Fricke, 1953; Asami et al., 1989; Beving et al., 1994; Gimsa et al., 1994, 1996).

In the fields of physics and electronics, resistor-capacitor (RC) models are commonly used to qualitatively describe relaxation processes and passive electrical properties. Although RC models were often used to describe special phenomena of cell polarization (Zhang and Willison, 1991; Jones, 1995), to the knowledge of the authors attempts to set up a consistent RC model are rarely published (Gimsa, 1997). This paper presents such a model, describing the two strong structural polarizations of the β dispersion range for the IMP of cell suspensions, as well as for DP, ER, the induced transmembrane potential, and cell-cell attraction. As a qualitative test, IMP and potentials obtained from the RC model are compared to the IMP of a human red cell suspension, the frequency behavior of dielectric membrane breakdown-induced hemolysis, as well as to DP and ER spectra.

This paper adresses researchers or students entering the field of IMP and electric field effects as well as experimentalists. The unified RC model offers easy access to the methods and to simple expressions for a qualitative interpretation of data or fast data fitting. Theoretical considerations allowed us to deduce a model geometry for which DP and ER behaviors are consistent with the spherical single-shell model. The simplicity of the model allows for a basic intuitive understanding of the interrelations of the methods and the influence of different cell parameters. It might therefore boost the still open detailed discussion of the advantages and shortcomings of the DP, ER, and IMP methods that was started by Wang et al. (1993).

MATERIALS AND METHODS

Cells

All experiments were carried out on washed human red cells at room temperature. An isotonic sucrose solution containing 1.5 mM phosphate buffer was used for IMP measurements. The cells were suspended at a hematocrit of 49% to avoid problems with an insufficient signal at low cell concentration. Because of this high cell concentration, ion displacement

and ion leakage from the cells raised the external conductivity to 0.12 S/m. For DP and ER, the cells were suspended at a hematocrit of 0.05%. To allow direct comparison of all methods, the conductivity was adjusted to 0.12 S/m by the addition of isotonic NaCl-phosphate buffer solution. All experiments were carried out at 23°C.

IMP

IMP characterization was conducted in a HP16452A liquid test fixture connected to an HP4194A impedance analyzer. Three different electrode distances (1.3 mm, 1.5 mm, and 2.0 mm) allowed us to eliminate electrode polarization effects. To that end, the IMP for a suspension layer of 1 mm thickness was calculated from the differences of all measured IMPs. For calculation, the actual electrode geometry of the test fixture was assumed (disc-shaped electrodes with a diameter of 38 mm).

AC field-induced cell hemolysis

Cell hemolysis was observed after a single AC pulse under an inverted microscope in a two-electrode chamber, which was mounted to a micromanipulator. The chamber electrodes were vertical platinum plates of 600 μm thickness at a distance of 60 μm. A pulse amplitude of 32 V_{PP} was used. The frequency was preadjusted on a HP8116A function generator (Hewlett Packard GmbH, Böblingen, Germany) that drove the chamber. A second HP8116A generator was used to release the pulse and to trigger the first generator for a pulse duration of 1 s. For experiments, cells were suspended at a hematocrit of 0.025% and an external conductivity of 0.12 S/m. At each frequency, survival rates of four different cell samples were determined. For each sample the fate of up to 27 cells and a minimum of 5 cells was recorded by VCR. Cells were counted as survivors when they did not lyse or lose their hemoglobin content within 1 min after the pulse.

DP and ER

To minimize electrolysis and heat production, a planar ultramicroelectrode chamber fabricated by semiconductor technology was used. The chamber had four electrodes at a separation of 200 μm (for details see Gimsa et al., 1996). It was driven by a computer-coupled 300-MHz generator (pulse generator HP8130A; Hewlett Packard GmbH) with 3 V_{pp} square-topped signals at a key ratio of 1:1. Four 90° phase-shifted signals were used to generate a rotating field. Complete spectra were measured by timing one rotation in (positive or cofield rotation) or against (negative or antifield rotation) the rotation direction of the field. The low hematocrit allowed the undistorted registration of single-cell movement. For DP, two neighboring electrodes were driven by signals of 180° phase shift. Dielectrophoretic cell translation was measured in the inhomogeneous field in the vicinity of one of the electrodes. The two critical frequencies for various external solution conductivities were determined by adjusting the frequency to the value at which cell movement ceased (for details see Gimsa et al., 1996). To obtain complete DP spectra, cells crossing a certain distance were timed when they moved toward (positive DP) or away from (negative DP) the electrode.

RESULTS

IMP

The IMP results are presented in two different ways. The real and imaginary parts of the complex IMP were plotted over the field frequency (Fig. 3 *A*) and in the complex plane (Cole-Cole plot; Fig. 3 *B*). A strong dispersion that is attributed to the membrane relaxation is clearly visible in the frequency range from 50 kHz to 3 MHz. The additional dispersion at frequencies below 1 kHz, which is especially pronounced in the Cole-Cole plot, must be attributed to the α-range. It was not further considered. Although the test fixture did not allow us to expand the frequency range beyond 15 MHz, a second β dispersion can be expected above 10 MHz (see the high-frequency part of the Cole-Cole plot).

Frequency dependence of AC field-induced cell hemolysis

To demonstrate the frequency dependence of the induced transmembrane potential, cell hemolysis experiments were carried out as described under Materials and Methods. The electrode distance used was an optimal value for the maximum voltage of the pulse of 32 V_{PP} available from the HP8116A function generator. For smaller interelectrode gaps, the number of observable cells was too small. At higher distances the applicable field strength became too low for dielectric membrane breakdown.

We are aware that our experimental criterion of the survival rate after 1 min is a very crude parameter, and not having lost hemoglobin within 1 min after the pulse is no criterion for actual survival of the cells. Nonetheless, the criterion is strongly correlated to the degree of field-induced membrane damage, which in turn is related to the induced transmembrane potential (Fig. 4 *A*).

DP and ER

In Fig. 4 *B* results of DP and ER measurements are presented independently. To plot experimental DP and ER values, the voltage scaling of the RC model (*left ordinate*) was used. To transform the measured data (*right ordinate*), the proportionality factors p and q were introduced. The ER spectrum exhibits an antifield rotation peak at low frequencies and a cofield rotation peak at higher ones. At the external conductivity used, DP spectra exhibit three different plateaus with two critical frequencies. DP and ER data were also plotted in the complex plane (Fig. 6). The p and q factors in Fig. 4 *B* were used.

In Fig. 5 the dependence of the two critical frequencies on the external conductivity is presented. The experimental data are from Gimsa et al. (1996). Above 0.5 S/m only negative DP was observed, which resulted in a merging of the two frequency branches.

DISCUSSION

Geometry of the model

Every cell was assumed to be surrounded by a cubical volume of suspension medium forming an elementary cube (Fig. 1). This geometry allowed us to model a cell suspension with elementary cubes in parallel and serial arrangement. Furthermore, a homogeneous external field applied by a pair of parallel electrodes was assumed. These electrodes were oriented parallel to the left and right sides of the

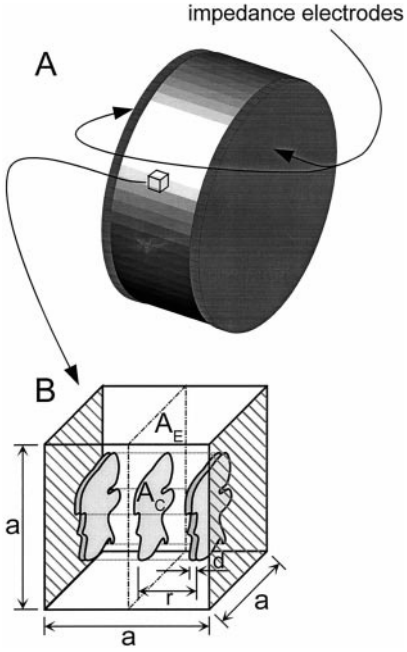

FIGURE 1 (*A*) Cell suspension in an IMP chamber (liquid test fixture HP16452A) split into elementary cubes. (*B*) Elementary cube containing the cell model. The center area of the cell is located in the symmetry plane of the elementary cube. The left and right sides of the cube are considered virtual electrodes (*hatched areas*). A_C, a, d, and r stand for the shadow area of the cell in field direction, the side length of the elementary cube, membrane thickness, and cell model radius, respectively. A_E is given by $a^2 - A_C$. Membrane areas perpendicular to the virtual electrode planes were neglected.

elementary cube. Thus these cube sides could be considered virtual electrodes. The RC model was deduced for a prismatic cell geometry limited by two parallel membrane planes of arbitrary but identical shape. These planes were oriented perpendicular to the normal direction of the field, shadowing each other. Thus the virtual electrodes and the symmetry plane of the elementary cube, as well as both sides of the membrane, could be considered equipotential planes. Membrane areas perpendicular to electrode areas were neglected because of their negligible contribution to the overall IMP. In this model any external field induces identical potentials of opposite signs at two points that are mirror-symmetrical to the symmetry plane of the elementary cube. Thus it is sufficient to put up a circuit model for only one-half of the elementary cube (Fig. 2).

Electric parameters of the model

The electric properties of every phase are determined by their capacitive and conductive properties (Fig. 2). The IMP Z^* for every homogeneous medium i between two equipotential planes of area A_i at a separation d_i is determined by the complex conductivity σ^*_i:

$$Z^*_i = \frac{1}{\sigma^*_i}\frac{d_i}{A_i} \tag{1}$$

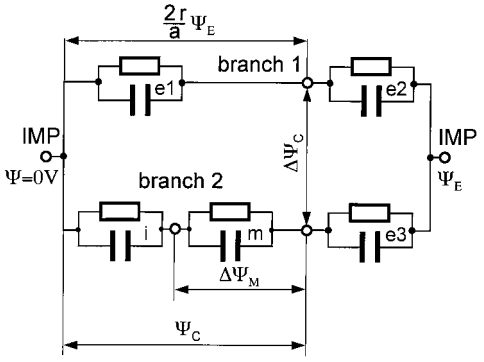

FIGURE 2 RC model for the right half of Fig. 1 *B*. The model consists of resistor-capacitor pairs according to Eqs. 1 and 2. Branch 1 summarizes the current path around the cell, and branch 2 represents the current path through the cell. The subdivision of branch 1 generates a reference potential in the external solution at a distance r from the symmetry plane. This reference potential exhibits no phase shift to the applied potential Ψ_E. Its amplitude is given by $(2r/a)\Psi_E$. $\Delta\Psi_M$ and $\Delta\Psi_C$ stand for the transmembrane and induced cell potentials, respectively (the difference in cell and suspension medium potentials).

where σ^*_i is given by

$$\sigma^*_i = \sigma_i + j\omega\epsilon_i\epsilon_0 \tag{2}$$

Here σ_i, j, ω, ϵ_i, and ϵ_0 stand for DC conductivity, $(-1)^{0.5}$, circular frequency, the relative permittivity, and the permittivity of vacuum. The above description is equivalent to a parallel circuit of a resistor and a capacitor of the same geometry, described by d_i and A_i, the values of which are determined by σ_i and ϵ_i, respectively. Three different media, the external and internal solutions and the membrane, were considered.

In the RC model the contributions of the external medium around the cell are summarized by branch 1. This branch is subdivided to generate a reference potential for the description of DP and ER. This reference potential is frequency independent. Branch 2 models the current flow over the cell. Its three RC pairs are formed by three media of prismatic shape possessing the same intersectional area. For a given geometry the values of all RC elements can easily be calculated from their permittivities and conductivities by Eqs. 1 and 2. Then the IMP of a cell suspension can most easily be deduced by applying Kirchhoff's laws to a meshwork consisting of pairs of the RC model that describes both halves of the elementary cube (see also Zhang and Willison, 1991):

$$\mathrm{IMP} = \frac{d_{el}/a}{A_{el}/a^2}(2*\mathrm{imp}) \tag{3}$$

Here imp, d_{el}, A_{el}, and a stand for the impedance of the RC scheme (Fig. 2), electrode distance, area of the test fixture, and the side length of the elementary cube (Fig. 1). For interpretation of the experimental IMP, realistic model dimensions and electrical parameters of the media were measured, calculated, or taken from the literature (Table 1). The numbers of parallel and serially switched RC schemes were

TABLE 1 Parameters used to calculate the parameters of the RC model from the model geometry

Geometrical parameters		
Hematocrit	49%	Measured
Cell volume; V	97 μm^3	Engström et al. (1992)
r	2.4 μm	Fitted
A_c	20.2 μm^2	Calculated from $V/(2r)$
a	5.8 μm	Calculated from hematocrit and cell volume
d	8 nm	Assumed
Conductivities		
External	σ_e = 0.12 S/m	Measured
Membrane	σ_m = 1 μS/m	Fricke (1925, 1953), Ballario et al. (1984), Asami et al. (1989), Bao et al. (1992), Gimsa et al. (1994, 1996)
Internal	σ_i = 0.53 S/m	Pauly and Schwan (1966), Georgiewa et al. (1989), Gimsa et al. (1996)
Relative permittivities		
External	ϵ_e = 80	
Membrane	ϵ_m = 9.04	Calculated from d and a specific membrane capacitance of 0.01 F/m^2 (Fricke, 1925, 1953; Arnold and Zimmermann, 1982; Gimsa et al., 1996)
Internal	ϵ_i = 50	Pauly and Schwan (1966)

calculated for fitting from the geometries of the test fixture and the elementary cube. All resistances and capacitances of the RC model were expressed for fitting by the model geometry in such a way that r and A_C could be varied without changing the model's hematocrit or cell volume. The side length a of the elementary cube was calculated from hematocrit and cell volume. Variation of the model cell geometry allowed us to fit the IMP as well as Real($\Delta\Psi_C$) and Imag($\Delta\Psi_C$) to the experimental points of IMP, DP, and ER measurements in parallel by eye. Fitted parameters are given in Table 1.

Interpretation of experiments by the RC model

When a potential difference is applied to a cell suspension modeled by elementary cubes according to Fig. 1 *B*, the potential at the symmetry planes will not change and, for reasons of symmetry, remains at the value that would be at this site in the absence of the cell. Thus this potential can be considered a reference potential or, for simplicity, 0 V. For an example calculation of the frequency dependence of induced potentials, a frequency-independent AC amplitude of Ψ_E = 1 V was assumed to be applied at the right side of the RC model (Fig. 2). This allows direct calculation of the frequency dependence of the transmembrane potential $\Delta\Psi_M$ (Fig. 4 *A*).

Furthermore, the frequency dependence of the model IMP can be obtained directly. Nonetheless, how is it possible to describe the mechanism of field-induced cell movements by an RC model? In contrast to IMP measurements, DP and ER do highlight differences in the polarizability of a single cell and its surroundings. These frequency-dependent differences cause the field-induced translational force and the torque in DP and ER, respectively. Usually DP and ER are modeled for an appropriate dielectric cell model by solving Laplace's equation for induced charges to obtain the overall induced dipole moment (Fuhr et al., 1985, 1986; Pastushenko et al., 1985; Sauer and Schloegl, 1985; Wang et al., 1993). Then the frequency dependence of ponderomotive force effects, the DP translation or ER rotation, can be calculated by taking into account the respective mechanism of interaction of the induced dipole moment with the external field.

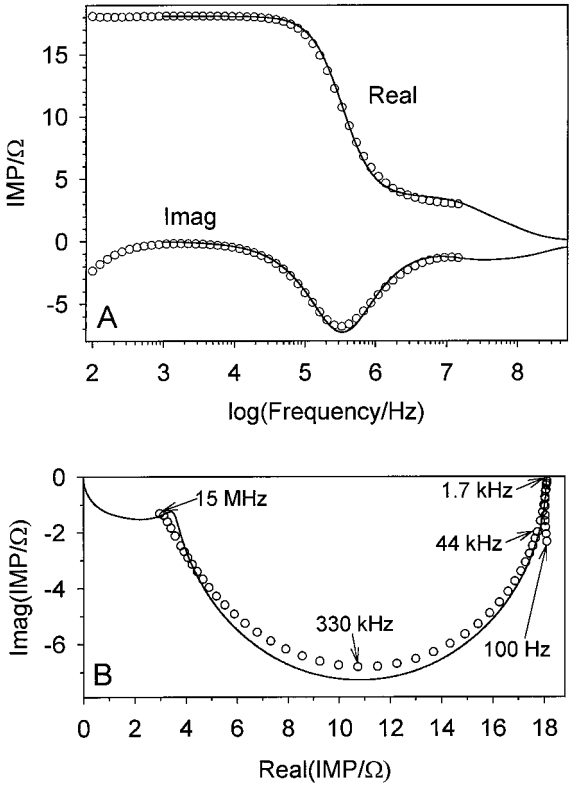

FIGURE 3 (*A*) Frequency dependence of real and imaginary parts of IMP. The points are measurements of the IMP of a red cell suspension. Curves were calculated according to the RC model of Fig. 2 (for parameters see Table 1). (*B*) Cole-Cole plot of *A*.

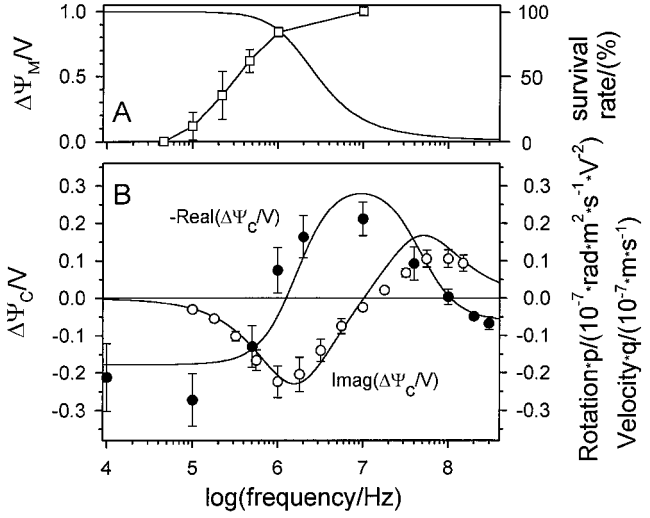

FIGURE 4 (*A*) Frequency dependence of the induced transmembrane potential, $\Delta\Psi_M$. The points are the survival rates of cells after breakdown pulses of different frequency (*right axis*). (*B*) Real and imaginary parts of $\Delta\Psi_C$, according to the model in Fig. 2 (for parameters, see Table 1). The points refer to the right ordinate. They are measurements of DP (*filled circles*) and ER (*open circles*). Theoretical curves refer to the left ordinate. The curves were calculated according to the RC model of Fig. 2. For DP and ER, proportionality coefficients for the different mechanisms of force generation and friction coefficients were introduced ($p = 0.75$, $q = 0.8$).

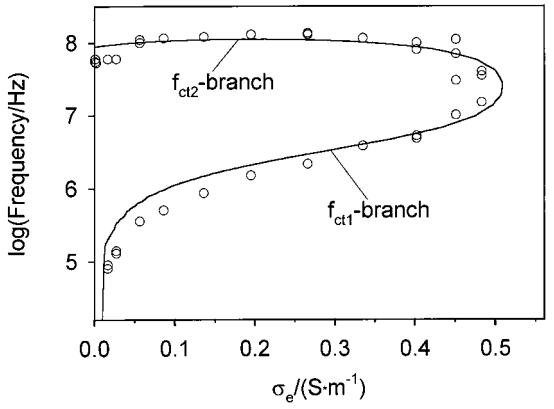

FIGURE 5 Critical frequencies of DP in dependence on the external conductivity. Measured points are from Gimsa et al. (1996). The curve was generated from the points where $|\text{Real}(\Delta\Psi_M)| = 0$. It exhibits a typical noselike shape with two branches for the first (f_{ct1}) and second (f_{ct2}) critical frequencies, respectively.

Fig. 4, *A* and *B*, compares the real and imaginary parts of the potential difference $\Delta\Psi_C$ with DP and ER measurements. The relation of the real and imaginary parts of the induced dipole moment to DP and ER, respectively, is a consequence of the mechanisms of the two methods. In DP cell translation is induced in an inhomogeneous AC field. A cell moves toward or away from regions of high field, depending on its polarizability relative to that of the suspension medium. In the RC model the balance of medium and cell polarizability is reflected by the potential difference $\Delta\Psi_C$ (Fig. 2). In DP as well as in ER, this potential difference is partly transformed into mechanical work. $\Delta\Psi_C$ can also be seen as the difference of the potentials that would exist at the site of the cell surface in the presence and the absence of the cell. Thus $\Delta\Psi_C$ reflects the energy change in the cell-medium system mediated by the displacement of the cell by the external medium or vice versa. This mechanism is obvious for the intercepts of the real part of $\Delta\Psi_C$ with the abscissa (Fig. 4 *B*). These intercepts correspond to the critical frequencies of DP, where the effective polarizabilities of the cell and the external medium are balanced and the DP force ceases (Fig. 5). For conductivities above a certain value, only negative DP can be observed, because the cell's polarizability does not reach the polarizability of the external medium for any frequency. Consequently, in a plot over the external conductivity, the two branches of the critical frequencies fuse with increasing conductivity.

The frequency dependence of the DP force is mediated by dispersions of the cell's polarizability. In a rotating field any dispersion process causes a spatial phase shift or slippage of the induced dipole moment and the external field. This is the prerequisite for a torque induced by the interaction of dipole moment and external field. The torque and therefore individual cell rotation is at maximum if the relaxation time of the dispersion process and external field frequency match. The reason is that the large amplitude of the induced dipole moment at lower frequencies does not effectively induce a torque because of its insufficient phase lag. At the opposite extreme, for frequencies that are too high, the phase lag will be closer to 90°, but the amplitude will have already declined. In other words, the resulting torque is proportional to the imaginary (out of phase) part of the induced dipole moment and can be calculated from the cross-product of the polarization and external field vectors (Pastushenko et al., 1985; Sauer and Schloegl, 1985; Gimsa et al., 1991a).

Frequency-dependent properties of the model

For frequencies so low that the capacitive resistance of the membrane is much higher than its ohmic resistance, the cell membrane represents a high IMP in the current branch 2 (Fig. 2). In this case the current mainly flows in branch 1, around the cell. The external membrane side of the cell will be charged to a potential close to Ψ_E. In analogy, the internal membrane side will be close to a potential of 0 V. Accordingly, the induced transmembrane potential $\Delta\Psi_M$ is at maximum.

The cell polarization is described by the potential of the external membrane side. This potential is much higher than it would be at the same site in the absence of a cell. The geometry was chosen such that this hypothetical potential corresponds to the potential at the branching of branch 1. For a suspended cell the potential difference $\Delta\Psi_C$ would generate a centripetal force that would be balanced by the other half of the cell in a homogeneous field. Only in an inhomogeneous field would a negative DP be observed, i.e.,

the system would favor a state in which the cell is displaced by the more polarizable external medium.

In an AC field, the described membrane polarization is a continuous recharging process. Its time constant is determined by the electrical properties of the external medium and the cell constituents. With increasing frequency, a phase shift of $\Delta\Psi_C$ to the external potential occurs if the membrane capacitance approaches the magnitude of the IMP of the e3 circuit. This is the process of membrane dispersion yielding the frequency dependence of the induced transmembrane potential $\Delta\Psi_M$ according to the Schwan equation for a spherical cell (Fig. 4 *A*; Fuhr et al., 1987; Marszalek et al., 1990; Grosse and Schwan, 1992):

$$\Delta\Psi_M = \frac{1.5rE}{\sqrt{1 + \left(\frac{\omega}{\omega_c}\right)^2}} \quad (4)$$

E, r, ω, and ω_c stand for the external field strength, the cell radius, the angular frequency of the external field, and the characteristic frequency of the membrane charging process, respectively. For the RC model, $1.5rE$ is given by Ψ_E.

In a rotating field the phase shift caused by the membrane-charging process would be expressed in an ER peak with the characteristic frequency ω_c. Because the induced charges at the cell's surface and the external field possess the same signs, the charges and therefore the cell would be pushed against the rotation direction of the external field (antifield rotation). From this mechanism the sensitivity of the peak for membrane properties is obvious.

At higher frequencies the membrane is capacitively bridged and the potentials will distribute according to the ohmic properties of the internal and external media. Because of the cytoplasmic conductivity, which is higher than the external conductivity, the internal side will be at a potential close to 0 V. The same applies to the external side of the membrane because of the low membrane IMP. Because the polarizability of the cell is now better than that of the external medium, it would travel toward areas of higher field strength in an inhomogeneous field (positive DP).

The contribution of the resistances to the potential distribution is frequency independent. Thus, with frequencies increasing even further, the polarization distribution becomes dominated by the capacitive properties of the media. A second dispersion ($\beta 2$) appears, and the potential over the cell becomes similar to that in the external solution, because the difference between the cytoplasmic and the external permittivity is low (Table 1). The $\beta 2$ dispersion again yields a phase shift between the applied potential and the potential at the cell surface, generating a torque in a rotating field. Because of the different signs of the induced charges and external field in this frequency range, cofield rotation is induced. Its mechanism makes the cofield peak especially sensitive to the cytoplasmic properties. Above the dispersion a third DP plateau is reached, which is determined by the permittivity differences of cytoplasm and external medium.

Fig. 6 presents the real and imaginary parts of the induced cell potential $\Delta\Psi_C$ in the complex plane. DP and ER measuring point pairs for the same frequencies were selected from Fig. 4 *B* (*top and right axes*). Vectors are drawn for a frequency of 1 MHz. $(2r/a)\Psi_E$ represents the frequency-independent reference potential, i.e., the potential difference between the symmetry plane and the reference point of branch 1. When this vector is used as the origin of a coordinate system, $\Delta\Psi_C$ sweeps all four quadrants. Two half-circles describe the dispersion of membrane capacitance (*lower arc*) and conductivity-based polarization (*top arc*), respectively.

The interaction force of two adjacent cells of the same properties is caused by the electrostatic interaction of their induced polarization charges. Although the magnitude of the force depends on the cell distance, the opposite poles of two cells will always attract, leading to pearl chain formation. Neglecting the influence of the polarization of one cell on the polarization of the other, the frequency dependence

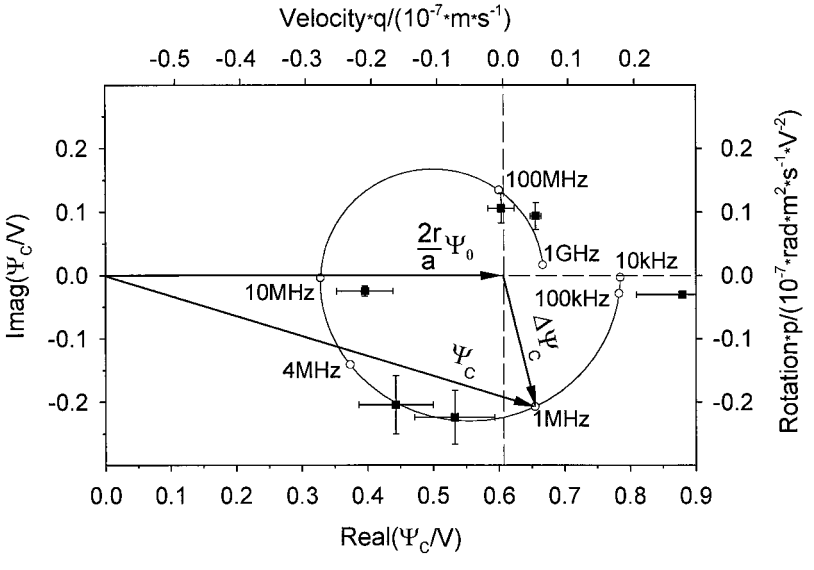

FIGURE 6 Cole-Cole plot of the real and imaginary parts of Ψ_C. Proportionality coefficients like those in Fig. 4 *B* were used. Certain frequencies of the theoretical curve are marked (○). The vectors depict the relations of Fig. 2 for a frequency of 1 MHz. Measured points for the same frequencies of DP and ER were selected from Fig. 4 *B* (■).

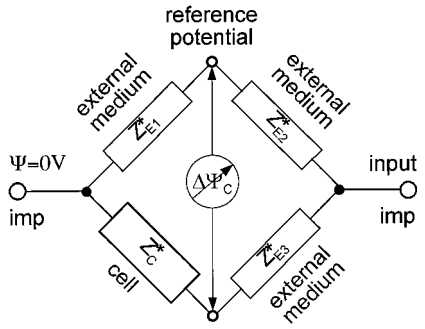

FIGURE 7 Redrawing of the RC model in Fig. 2. The figure demonstrates the Wheatstone bridge-like principle of the single cell methods DP and ER. Z^*_{E1}, Z^*_{E2}, and Z^*_{E3} stand for the IMPs of the three RC pairs e1, e2, e3, respectively, which describe the external solution. Z^*_C stands for the IMP of the cell (RC pairs i and m; see Fig. 2).

of the attraction force can easily be deduced from the amplitude of $|\Delta\Psi_C|$.

Shortcomings of the model

Although experiments and calculations for IMP, DP, and ER were conducted at completely different cell concentrations, all measurements and theoretical curves are amazingly consistent. Nonetheless, when we calculated DP and ER for very low model hematrocrit values, we found that the first characteristic frequency drastically shifted toward low frequencies. This behavior occurred because the time constant of membrane polarization, for a negligible membrane conductivity given by

$$\tau = (R_i + R_{e3})C_m. \quad (5)$$

τ is strongly influenced by resistor e3. The value of this resistor increases drastically with decreasing hematocrit. This result is an erroneous reflection of the actual relations, in which the characteristic frequency of ER is independent of the amount of the surrounding medium. In contrast, the characteristic frequency of dispersion of IMP depends on cell concentration (Wang et al., 1993). These considerations suggest that the striking correspondence of our experimental and theoretical IMP, DP, and ER results is due to the special geometry of our elementary cube (Fig. 1 and Table 1).

Capabilities and potencies of the model

A correct model must take into account the fact that polarization disturbs the field only in the vicinity of a single cell. It must be assumed that the radius to which the disturbance projects into the suspension medium depends on polarizability and is characteristic for a certain cell shape. In the RC model these relations can be described by the introduction of an "influential radius" r_{infl}, which is of course larger than the "cell radius" r (compare to Fig. 1). r_{infl} would determine the point where the current branches 1 and 2 split. Thus r_{infl} is given by half the side length of the elementary cube, $a/2$, which corresponds to the right point of Fig. 2. How can the correct r_{infl} be found for a given cell geometry, e.g., for a sphere? For the extreme case of no membrane conductivity, and a high external and a very high internal conductivity, the real part of $\Delta\Psi_C$ corresponds to the voltage over e2 at low and to that over e1 for medium frequencies, where the membrane is completely polarized or capacitively bridged, respectively. For a single-shell sphere, these two cases are reflected by a Clausius-Mossotti factor of -0.5 and 1, respectively (compare to Appendix A in Gimsa et al., 1991b). The RC model would reflect these relations for $a = r_{infl} = 1.5r$. Assuming this value for the geometry of Fig. 1 *B* and simplified electric schemes for the limiting cases in the different frequency ranges (see discussion on the frequency-dependent properties of the model) allows us to put up equations for Ψ_C, $\Delta\Psi_C$, and $\Delta\Psi_M$. They can easily be solved, leading, e.g., to Eq. 4 or to expressions for characteristic points of DP and ER spectra (see Appendix A of Gimsa et al., 1991b). For example, solving Eq. 5 immediately leads to the well-known expression for the first characteristic frequency of ER. Such simplified equations are not only of importance for understanding the basic parameter dependencies of DP and ER, but also for fast nonlinear fitting of experimental data. Starting from the full single-shell model, these results could only be obtained after extensive calculations on the basis of row developments after the introduction of area-specific parameters for the membrane (Gimsa et al., 1991b). The surprising consistency of the spherical single-shell model with an RC model of prismatic geometry and $r_{infl} = 1.5r$ suggests that our different simplifications compensated for each other.

The IMP of a suspension exhibits a cell concentration dependence (Wang et al., 1993). Therefore, the introduction of an influential radius for IMP modeling was not necessary. In our case the side length, a, of the elementary cube was $1.2r$ because of our high hematocrit (Table 1). Thus r_{infl} and, accordingly, the resistor e3 were too low, shifting the theoretical frequency dependencies of DP, ER, and the induced transmembrane potential curves.

The influential radius of $1.5r$ also works for the homogeneous sphere model. The potencies of the concept for other model geometries like ellipsoids and cylinders was not yet investigated. Most probably values for a correct description can be found and tested by comparison to existing models (Pastushenko et al., 1985; Sauer and Schloegl, 1985; Fuhr et al., 1986; Müller et al., 1990; Paul and Otwinowski, 1991). If this could be achieved, RC models would allow easy access to more complex geometries, certain patterns in the electric properties of membrane and cytoplasm, etc.

CONCLUSIONS

The RC model makes it possible to describe structural Maxwell-Wagner dispersions and explains the interdependencies of IMP, induced transmembrane potential, DP, and ER in a suggestive manner. The model may also offer a

simple approach to the explanation of cell orientation, deformation, and pearl-chain formation. Obviously, no resonance circuit is necessary to explain ER, showing that Pohl's term, "cellular spin resonance," is inadequate (Pohl, 1983). The superior resolution of the single-cell methods over conventional IMP is not only demonstrated by the fact that the measuring effect of IMP, in contrast to DP or ER, decreases with decreasing cell concentration, but also by the following consideration: the potential difference $\Delta\Psi_C$ can be considered as the measuring signal of a Wheatstone bridge consisting of the two branches of Fig. 2. Because the measuring effects of DP and ER are based on the differential bridge signal $\Delta\Psi_C$, these methods are more sensitive for registration of cell properties. Another consequence of the differential principle is that the Cole-Cole plots of the single-cell methods sweep all four quadrants, whereas the IMP plot sweeps only one (Figs. 3 *B* and 6; Fuhr et al., 1985; Wang et al., 1993). The influential radius concept allows the deduction of simplified equations for the critical and characteristic frequencies, force plateaus, and peak heigths of DP and ER for the spherical single-shell model. We believe that a detailed discussion of the advantages and shortcomings of the DP, ER, and IMP methods based on a unified theory is still open and hope that the RC approach may boost this discussion.

We are grateful to Ms. Ch. Mrosek for technical assistance and to Drs. G. Risuleo and A. Bonincontro for stimulating discussions. Dr. U. Gimsa is acknowledged for help with the manuscript.

This work was supported by grants DAAD 314-Vigoni-dr and DFG Gi 232/1-2.

REFERENCES

Ackmann, J. J., and M. A. Seitz. 1984. Methods of complex impedance measurements in biologic tissue. *CRC Crit. Rev. Biomed. Eng.* 11: 281–311.

Arnold, W. M., B. M. Geier, B. Wendt, and U. Zimmermann. 1986. The change in the electro-rotation of yeast cells effected by silver ions. *Biochim. Biophys. Acta.* 885:35–48.

Arnold, W. M., and U. Zimmermann. 1982. Rotating-field-induced rotation and measurement of the membrane capacitance of single mesophyll cells of *Avena sativa. Z. Naturforsch.* 37c:908–915.

Asami, K., Y. Takahashi, and S. Takashima. 1989. Dielectric properties of mouse lymphocytes and erythrocytes. *Biochim. Biophys. Acta.* 1010: 49–55.

Asami, K., and T. Yonezawa. 1996. Dielectric behavior of wild-type yeast and vacuole-deficient mutant over a frequency range of 10 kHz to 10 GHz. *Biophys. J.* 71:2192–2200.

Ballario, C., A. Bonincontro, C. Cametti, A. Rosi, and L. Sportelli. 1984. Effect of alkali metal salts on the electric parameters of human erythrocytes in normal and pathological conditions (homozygous β-thalassemia). *Z. Naturforsch.* 39c:1163–1169.

Bao, J. Z., C. C. Davis, and R. E. Schmukler. 1992. Frequency domain impedance measurements of erythrocytes. *Biophys. J.* 61:1427–1434.

Beving, H., L. E. G. Eriksson, C. L. Davey, and D. B. Kell. 1994. Dielectric properties of human blood and erythrocytes at radio frequencies (0.2–10 MHz); dependence on cell volume fraction and medium composition. *Eur. Biophys. J.* 23:207–215.

Burt, J. P. H., R. Pethig, P. R. C. Gascoyne, and F. F. Becker. 1990. Dielectrophoretic characterisation of Friend murine erythroleukaemic cells as a measure of induced differentiation. *Biochim. Biophys. Acta.* 1034:93–101.

Crane, J. S., and H. A. Pohl. 1972. Theoretical models of cellular dielectrophoresis. *J. Theor. Biol.* 37:15–41.

Donath, E., V. Pastushenko, and M. Egger. 1990. Dielectric behaviour of the anion-exchange protein of human red blood cells—theoretical analysis and comparison to electrorotation data. *Bioelectrochem. Bioenerg.* 23:337–360.

Engström, K. G., B. Möller, and H. J. Meiselman. 1992. Optical evaluation of red blood cell geometry using micropipette aspiration. *Blood Cells.* 8:241–258.

Fricke, H. 1925. The electric capacity of suspensions with special reference to blood. *J. Gen. Physiol.* 9:137–152.

Fricke, H. 1953. Relation of the permittivity of biological cell suspensions to fractional cell volume. *Nature.* 172:731–732.

Fuhr, G., J. Gimsa, and R. Glaser. 1985. Interpretation of electrorotation of protoplasts. I. Theoretical considerations. *Stud. Biophys.* 108:149–164.

Fuhr, G., R. Glaser, and R. Hagedorn. 1986. Rotation of dielectrics in a rotating electric high-frequency field. Model experiments and theoretical explanation of the rotation effect of living cells. *Biophys. J.* 49:395–402.

Fuhr, G., R. Hagedorn, R. Glaser, J. Gimsa, and T. Müller. 1987. Membrane potentials induced by external electric fields. *J. Bioelectricity.* 6:49–69.

Fuhr, G., and P. I. Kuzmin. 1986. Behavior of cells in rotating electric fields with account to surface charges and cell structures. *Biophys. J.* 50:789–795.

Fuhr, G., P. Rösch, T. Müller, V. Dressler, and H. Göring. 1990. Dielectric spectroscopy of chloroplasts isolated from higher plants - characterization of the double-membrane system. *Plant Cell. Physiol.* 31:975–985.

Gascoyne, P. R. C., F. F. Becker, and X.-B. Wang. 1995. Numerical analysis of the influence of experimental conditions on the accuracy of dielectric parameters derived from electrorotation measurements. *Bioelectrochem. Bioenerg.* 36:115–125.

Geier, B. M., B. Wendt, W. M. Arnold, and U. Zimmermann. 1987. The effect of mercuric salts on the electro-rotation of yeast cells and comparison with a theoretical model. *Biochim. Biophys. Acta.* 900:45–55.

Georgiewa, R., E. Donath, and R. Glaser. 1989. On the determination of human erythrocyte intracellular conductivity by means of electrorotation—influence of osmotic pressure. *Stud. Biophys.* 133:185–197.

Georgiewa, R., B. Neu, V. M. Shilov, E. Knippel, A. Budde, R. Latza, E. Donath, H. Kiesewetter, and H. Bäumler. 1998. Low frequency electrorotation of fixed red blood cells. *Biophys. J.* 14:2114–2120.

Gimsa, J. 1997. Dielektrische Charaterisierung und Manipulation von Partikeln und biogischen Zellen. Habilitation thesis. Humboldt-Universität zu Berlin.

Gimsa, J., R. Glaser, and G. Fuhr. 1991a. Theory and application of the rotation of biological cells in rotating electric fields (electrorotation). *In* Physical Characterization of Biological Cells. W. Schütt, H. Klinkmann, I. Lamprecht, and T. Wilson, editors. Verlag Gesundheit, Berlin. 295–323.

Gimsa, J., P. Marszalek, U. Löwe, and T. Y. Tsong. 1991b. Dielectophoresis and electrorotation of neurospora slime and murine myeloma cells. *Biophys. J.* 60:5–14.

Gimsa, J., T. Müller, T. Schnelle, and G. Fuhr. 1996. Dielectric spectroscopy of single human erythrocytes at physiological ionic strength: dispersion of the cytoplasm. *Biophys. J.* 71:495–506.

Gimsa, J., T. Schnelle, G. Zechel, and R. Glaser. 1994. Dielectric spectroscopy of human erythrocytes: investigations under the influence of nystatin. *Biophys. J.* 66:1244–1253.

Grosse, C., and H. P. Schwan. 1992. Cellular membrane potentials induced by alternating fields. *Biophys. J.* 63:1632–1642.

Hölzel, R. 1997. Electrorotation of single yeast cells at frequencies between 100 Hz and 1.6 GHz. *Biophys. J.* 73:1103–1109.

Jones, T. B. 1995. Electromechanics of Particles. Cambridge University Press, Cambridge, New York, and Melbourne.

Kaler, K. V. I. S., and T. B. Jones. 1990. Dielectrophoretic spectra of single cells determined by feedback-controlled levitation. *Biophys. J.* 57: 173–182.

Lisin, R., B. Z. Ginzburg, M. Schlesinger, and Y. Feldman. 1996. Time domain dielectric spectroscopy study of human cells. I. Erythrocytes and ghosts. *Biochim. Biophys. Acta.* 1280:34–40.

Marszalek, P., D.-S. Liu, and T. Y. Tsong. 1990. Schwan equation and transmembrane potential induced by alternating electric field. *Biophys. J.* 58:1053–1058.

Müller, T., G. Fuhr, F. Geissler, and R. Hagedorn. 1990. Rotation spectra of mouse eggs up to 35 MHz: experiments and theoretical interpretation. *Stud. Biophys.* 139:77–94.

O'Konski, C. T. 1960. Electric properties of macromolecules. V. Theory of ionic polarization in polyelectrolytes. *J. Phys. Chem.* 64:605–619.

Pastushenko, V. Ph., P. I. Kuzmin, and Yu. A. Chizmadshev. 1985. Dielectrophoresis and electrorotation: a unified theory of spherically symmetrical cells. *Stud. Biophys.* 110:51–57.

Paul, R., K. V. I. S. Kaler, and T. B. Jones. 1993. A nonequilibrium statistical mechanical calculation of the surface conductance of the electrical double layer of biological cells and its application to dielectrophoresis. *J. Phys. Chem.* 97:4745–4755.

Paul, R., and M. Otwinowski. 1991. The theory of the frequency response of ellipsoidal biological cells in rotating electrical fields. *J. Theor. Biol.* 148:495–519.

Pauly, H., and H. P. Schwan. 1959. Über die Impedanz einer Suspension von kugelförmigen Teilchen mit einer Schale. *Z. Naturforsch.* 14b: 125–131.

Pauly, H., and H. P. Schwan. 1966. Dielectric properties and ion mobility in erythrocytes. *Biophys. J.* 6:621–639.

Pethig, R., and D. B. Kell. 1987. The passive electrical properties of biological systems: their significance in physiology, biophysics and biotechnology. *Phys. Med. Biol.* 32:933–977.

Pohl, H. A. 1978. Dielectrophoresis. The Behavior of Neutral Matter in Nonuniform Electric Fields. Cambridge University Press, Cambridge, London, New York, and Melbourne.

Pohl, H. 1983. Cellular spin resonance: a new method for determining the dielectric properties of living cells. *Int. J. Quantum Chem.* 10:161–174.

Sauer, F. A., and R. N. Schloegl. 1985. Torques exerted on cylinders and spheres by external electromagnetic fields. A contribution to the theory of field-induced cell rotation. *In* Interactions Between Electromagnetic Fields and Cells. A. Chiabrera, C. Nicolini, and H. P. Schwan, editors. Plenum Press, New York. 203–251.

Schwan, H. P. 1957. Electrical properties of tissue and cell suspensions. *In* Advances in Biological and Medical Physics. J. H. Lawrence and C. A. Tobias, editors. Academy Press, New York. 147–209.

Schwan, H. P., and S. Takashima. 1993. Electrical conduction and dielectric behavior in biological systems. *In* Encyclopedia of Applied Physics, Vol. 5. VCH Publishers, Weinheim and New York. 177–200.

Sukhorukov, V. L., and U. Zimmermann. 1996. Electrorotation of erythrocytes treated with dipicrylamine: mobile charges within the membrane show their "signature" in rotational spectra. *J. Membr. Biol.* 153:161–169.

Takashima, S., and K. Asami. 1993. Calculation and measurement of the dipole moment of small proteins: use of protein data base. *Biopolymers.* 33:59–68.

Wang, X.-B., Y. Huang, P. R. C. Gascoyne, F. F. Becker, R. Hölzel, and R. Pethig. 1994. Changes in Friend murine erythroleukaemia cell membranes during induced differentiation determined by electrorotation. *Biochim. Biophys. Acta.* 1193:330–344.

Wang, X.-B., Y. Huang, R. Hölzel, J. P. H. Burt, and R. Pethig. 1993. Theoretical and experimental investigations of the interdependence of the dielectric, dielectrophoretic and electrorotational behaviour of colloidal particles. *J. Phys. D. Appl. Phys.* 26:312–322.

Zhang, M. I. N., and J. H. M. Willison. 1991. Electrical impedance analysis in plant tissue: a double shell model. *J. Exp. Bot.* 42:1465–1475.

Zimmermann, U., and W. M. Arnold. 1983. The interpretation and use of the rotation of biological cells. *In* Coherent Excitations in Biological Systems. H. Fröhlich and F. Kremer, editors. Springer-Verlag, Berlin. 211–221.